Electrical Fault Isolation and Signal Mapping in 3D IC

J. Gaudestad, A. Orozco
Neocera, LLC, 10000 Virginia Manor Road, Beltsville, MD, 20705, USA

1. Abstract

Magnetic Field Imaging has two major applications; Space Domain Reflectometry for Opens detection and Magnetic Current Imaging for shorts and leakage detection in addition to advanced signal mapping and path finding. We show that these techniques together can be a potential one-stop solution for all static Electric Fault Isolation in 3D devices where accurate information in all three dimensions is needed to analyze and test stacked 3D ICs with Through Silicon Via chains.

Keywords: Open, short, Magnetic Field Imaging, MFI, Space Domain Reflectometry, SDR, Magnetic Current Imaging, MCI, 3D, TSV

1. Introduction

Driven by strong demand for smart phones and tablets, the semiconductor industry needs to increase data speed transfer while preserving signal integrity between dies; all the while consuming less power [1]. The solution to achieve this has been to move towards 2.5D and 3D Integrated Circuits (IC), a solution that will allow companies to create devices that far exceed Moore's Law [2].

2.5D IC is a System in Package (SiP) where the dies are connected to the substrate through a passive silicon interposer (active-on-passive) with Through Silicon Vias (TSVs) connecting the metallization layers on its upper and lower surfaces [3]. 3D ICs, on the other hand, will stack two or more dies (active-on-active) on top of each other using TSV technology by stacking the chips normally placed on a Printed Circuit Board (PCB) in one device [2].

In this paper we first show a case study where an open is localized in X and Y using SDR and then finding the Z distance to the fault location using a simple 3D analysis on a long straight signal path [16]. This 3D analysis is expanded to a more advanced algorithm using 3D solver to make MFI also applicable for advanced 3D ICs with TSV chains [17].

2. Magnetic Field Imaging (MFI)

Magnetic Field Imaging (MFI) is based on mapping the magnetic field produced by a signal injected into the failing structure of the device under test (DUT). Unlike optical radiation employed by Electrical Fault Isolation (EFI) techniques such as thermal and photon emission [4, 5, 6], the magnetic field has the advantage of passing unperturbed through virtually any material used in semiconductor manufacturing. The magnetic field image of the DUT is converted into current density image by using a Fourier Transform inversion technique [7, 8]. In order to determine the fault location or signal path, the current image is superimposed onto an optical image usually acquired with a near infrared (NIR) camera.

MFI has two major implementations: Magnetic Current Imaging (MCI) for localization of shorts and leakages in addition to 3D TSV analysis and path finding [9] and Space Domain Reflectometry (SDR) for localization of open defects [10]. For MCI applications, magnetic field is imaged by either a Superconducting Quantum Interference Device (SQUID) or Giant Magneto Resistive (GMR) sensors. The SQUID sensor is mostly applicable for package level devices with working distances beyond 100µm and/or when low current is required. Alternating currents (AC) at 2-15 kHz provide for noise reduction using a lock-in amplifier. The GMR sensor is used for the front side wafer/die level high resolution (submicron) imaging using AC sampling currents at 95 kHz [11]. In SDR applications the SQUID detects a radio frequency (~40MHz) current forming a standing wave in the open trace [12].

SQUID and GMR sensors differ in both sensitivity and spatial resolution. SQUID is the most sensitive magnetic sensor known [11], and for electronic fault isolation it is typically used to image AC sine currents as low as 500 $\mathrm{nA}_{\mathrm{peak-to-peak}}$ ($3.125 \cdot 10^{-15}$ $\mathrm{Watt}_{\mathrm{rms}}$ at 1Ω resistance) at a working distance of several hundred microns between the current path and sensor (Converting sine AC peak to peak current to root mean square (rms), the current needs to be divided by $2 \cdot \sqrt{2}$). The SQUID sensor is kept in vacuum at cryogenic temperature, while the DUT is raster-scanned at room temperature and separated from the SQUID sensor enclosure by a thin diamond window. This setup allows localizing currents to within ±3 microns.

3. 3D modeling of magnetic fields

In a generalized form, the Biot-Savart Law can be written as:

$$\vec{B}(\vec{r}) = \frac{\mu_0 I}{4\pi} \oint \frac{d\vec{l} \times \vec{r}}{|\vec{r}|^3} \qquad (1)$$

where $\vec{B}$ is the magnetic induction, $= 4\pi 10^{-7}\ T \cdot m/A$ is the vacuum permeability, $d\vec{l}$ is the current carrying displacement vector, $\vec{r}$ is the vector from the origin to the SQUID, and I is the current magnitude [7]. For an infinitely long wire ($l \to \infty$), and using the fact that our magnetic sensors only detect the z-component of the magnetic field (B_z), one obtains a simplified version of Eq. 1:

$$B_z(y,z) = \frac{\mu_0 I}{4\pi} \cdot \frac{2y}{y^2 + z^2} \qquad (2)$$

If we plot the z component of the magnetic field when the sensor is in a constant plane above the current trace, one gets the profile as shown in Fig. 1. In this case the current trace is going straight "in to the paper" and located at origin.

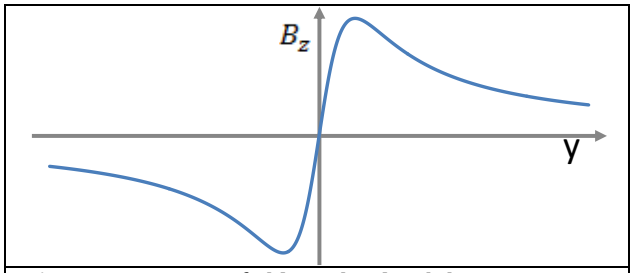

Figure 1. *Magnetic field amplitude while scanning in y direction using Equation 3*

The profile of the magnetic field of a line scan across a straight current trace has two extreme points. To find these extreme points we need to take the partial derivative of B_z with respect to y and equal this result to zero and one obtains the simple solution:

$$y_{minimum-to-maximum} = 2z \qquad (3)$$

The result in Equation 3 reveals that the distance from origin to the y location of any of the extreme points of the magnetic field (Fig. 1) is identical to the z-distance from the sensor to the current carrying trace, or that the distance between the extreme points horizontally is equal to twice the distance from the sensor to the current carrying trace (Equation 3). This result can be used to very accurately calculate the z-distance in a 3D integrated circuit.

4. Case Study 1: Double Stacked micro bumps with open defect [16]

A 2.5D test sample with no active components have two dies connected using micro bumps in a sandwich-like buildup with the metal layers in between the two dies (Fig. 3). The bottom die of the double stack is 26×24mm in size, while the top three dies form a rectangular shape of 24×22mm in size, exposing the 2-mm-wide edge of the bottom die for probing, where the test pads of 40×60µm in size enable for electrical connections to the daisy chains. The micro bumps have a diameter of 45µm (Fig. 2). The bottom die had full thickness silicon of 725µm, however the top die had been thinned to approximately 500um.

Electrical testing showed that the defective double stacked die sample had 720kΩ resistance between probe point A and probe point B (Yellow path in Fig. 2) while a good comparable sample had 4kΩ resistance between the same probe points.

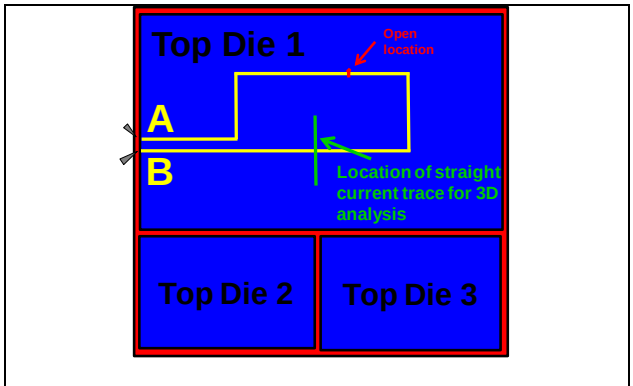

Figure 2. *Top view of the double stacked die. The bottom die (red) has three dies on top (blue). The Top Die 1 has a Daisy Chain (yellow path) with a cracked micro bump. The RF probes are connected to the bottom die.*

A 60MHz signal was injected into probe point B and SDR was performed on the sample (Fig. 3).

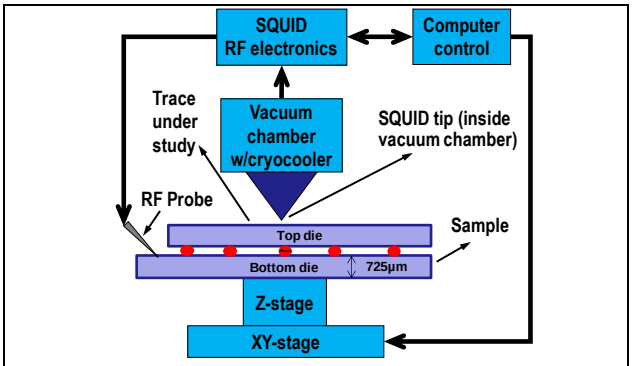

Figure 3. *The SQUID is under vacuum while the sample is un room temperature on top of am XY stage. RF Probers inject the RF signal onto the sample under test.*

The SDR results showed a clear and decaying signal towards the open location according to the Linear Decay Theory [10]. The SDR image was overlaid the optical image for accurate fault isolation (Fig. 4).

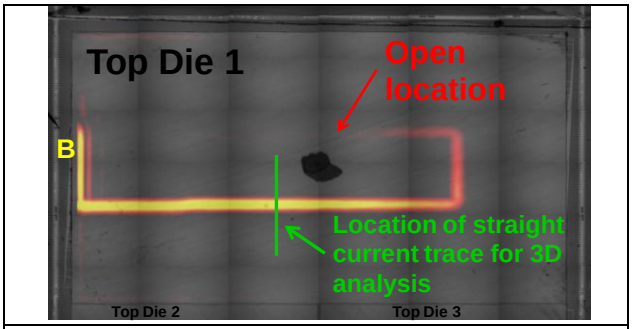

Figure 4. *Probe point B having RF signal showing reflection at open location*

Fig. 4 shows the RF signal injected from test point B and leaving the other test point A (shown in Fig. 2) floating (it does not need to be grounded). The open location is where the RF signal decays to zero (displayed by red arrow in Fig. 4) and was found using Linear Decay Analysis and confirmed using 2D XRay. The open was due to two separated micro bumps, causing poor connection with a large enough impedance change to cause signal reflection [13].

4.1 3D Analysis using Magnetic Field

The data shown in Fig. 4 has a long straight signal trace that can be used to find the Z distance using equation 3. The signal image in Fig. 4 is based on raw magnetic field data shown in Fig. 5.

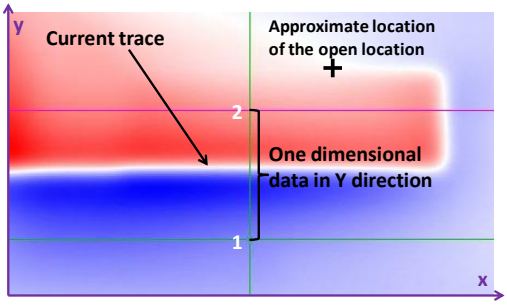

Figure 5. *The magnetic field image used for the total z-distance analysis to find the SQUID-to-Current Trace distance.*

If taking a line cut across a straight current carrying trace between point 1 and 2 in Fig. 5, one will get a profile as shown in Fig. 3. Fig. 6 shows the actual raw data line cut between point 1 and 2 shown in Fig. 5.

A data analysis algorithm is used to find the location of the minimum and the maximum point on the y-axis. When the distance between the two extreme data points of the magnetic field has been found, one can use Eq. 3 for a single line of data to find the total z-distance.

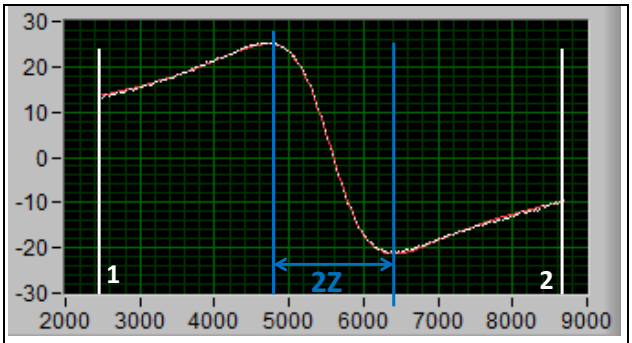

Figure 6. *Shows the raw magnetic field line data (white) and the theoretical line data (red) overlaid to calculate the distance between the two extreme points.*

The algorithm calculations found that the distance between the surfaces of the sample to the signal path was 525 µm. After checking the thickness of the top die using an accurate Touch Probe, the die was found to be slightly thicker than 500 µm.

4.2 Case Study 1: Conclusion

We showed that it is possible to use MFI with a high frequency SQUID using SDR to find the XY location of the open defect to the correct microbump (45µm), and then perform additional 3D analysis to find the z-distance from the surface of the sample to the signal trace with an accuracy of better than 25µm. SDR has shown to be repeatable of finding the open location to within 30µm in XY location.

5. Case Study 2: Advanced magnetic field imaging of TSV 3D IC [17]

A serious limitation with the standard inversion technique is that, in order to compute the current based on the acquired magnetic data, it is assumed that all currents are confined to a single plane. For that reason, to obtain the 3D current path in a Device under Test (DUT) one needs a new solver algorithm capable of going beyond the two-dimensional constraints and extract 3D information [17].

5.1 The Magnetic Field 3D Solver

A solver algorithm capable of successfully reconstructing a 3D current path based on an acquired magnetic field image has been developed. The generic 3D inverse problem has no unique solution (Equation 1). Given a particular 3D magnetic field distribution, there are an infinite number of current path distributions that will result in such magnetic field. This ill-posed problem has restricted, so far, the use of magnetic imaging to 2D. A different kind of 3D solver can be constructed, nevertheless capable of obtaining a single solution. One key to success is the selection of reasonable constraints that are compatible with typical current distributions in integrated circuits and packages. For example, current is mainly contained in layers and each layer is connected vertically. Similarly we impose Manhattan geometry restrictions on the current paths. This second constraint can be relaxed to allow other geometrical path configurations but it has proven to be generic enough. A second key ingredient is a starting current path that is not far from the correct solution. This is not trivial but we have found that the magnetic field image itself can be used to determine a "good-enough" starting path that allows for the convergence of the solution. The ultimate limits of the resolution capability depend in a complex manner on different system and scan parameters such as canning distance and noise in the image. These are the most important factors affecting lateral and vertical resolution.

The 3D solver algorithm is not only capable of extracting the 3D current path but it also provides valuable geometrical information about the device in X, Y and Z direction. It can also determine the distance below the sample surface that the top-most current is located and thus, provides in a multi-layer or stacked-die device which particular layer (or die) the defect is located at [14]. As stated above, the limitations of the technique in terms of lateral (XY) and vertical (Z) resolution as well as the number of dies it can resolve depend in a complex way on many factors and its discussion is beyond the scope of this paper (see [14] for a brief discussion).

5.2 IMEC stacked Die sample

A double stacked die, provided by IMEC, with a full thickness 775µm die at the bottom and a thinned 50µm die on top of the substrate die was connected using micro bumps and Through Silicon Vias (TSVs) (see Fig. 7). The structure we will focus on is a daisy chain with two interwoven 20µm-pitch daisy chain. The goal of this study is to test the 3D capability of magnetic field imaging using the newly developed 3D solver technique. Figure 7a shows the CAD image of both bottom and top dies with the pad probing area marked by the yellow rectangle and the area containing the daisy chain structure in the red rectangle. Figure 7b shows a cross-section sketch of the two dies and the micro-bump interconnect. Finally, Figure 7c shows a 3D rendering of the daisy chain structure with top die connections in orange and bottom ones in blue. Note that some of the traces connect top pads while others connect bottom ones. Also, note the alternating nature of the connection. This particular structure is of special interest as it contains TSVs and is a fairly complex path

meandering among 2 daisy chain structures and also combines small (1-2 mm) metal traces and large TSV pads (about 15 mm length).

Magnetic field images were acquired with a commercial system. The system consists of two sensors, a Superconducting Quantum Interference Device (SQUID) and a giant-magnetoresistance (GMR) sensor in a single platform, along with a near infra red (NIR) camera that allows acquiring optical image of the same area scanned under the magnetic sensors. This allows to registration of the magnetic images with the optical image for physical localization on the device and also seamless scanning of the same area under the SQUID and/or the GMR sensors. As the SQUID sensor needs to be in the superconducting state to operate, it needs to be cooled at about 77K and it is kept in vacuum inside an enclosure separated from the sample which remains at room temperature and in air. This forces a minimum separation distance between the SQUID sensor inside the vacuum chamber and the surface of the sample, on the outside. This scanning distance ultimately limits the resolution of the SQUID images to about ±3µm at best under typical scanning conditions. The GMR sensor, on the other hand, operates at room temperature and it is of much smaller size, allowing to scan in soft contact with the sample surface and thus, increasing the resolution of the scan, allowing for submicron resolution for front access. This technique is widely used today in the semiconductor industry and a review can be found in [15].

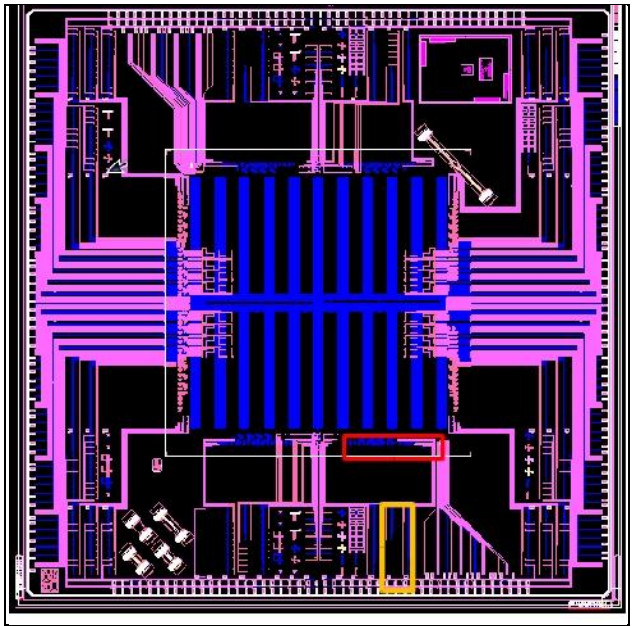

Figure 7a. *CAD image of both bottom and top dies with the pad probing area marked by the yellow rectangle and the area containing the daisy chain structure in the red rectangle.*

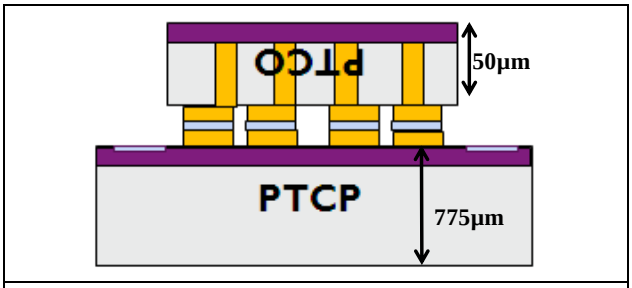

Figure 7b. *Cross-section sketch of the two dies and the micro-bump interconnects.*

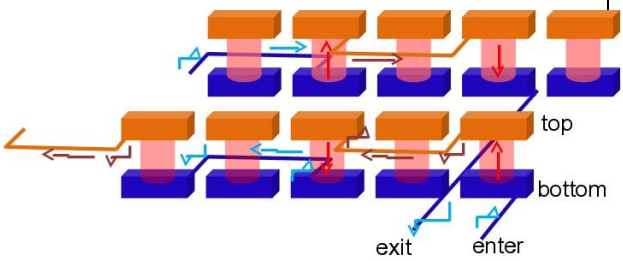

Figure 7c. *3D rendering of the daisy chain structure with top die connections in orange and bottom ones in blue. Note that some of the traces connect top pads while others connect bottom ones. Also, note the alternating nature of the connection.*

Figure 7 (c) 3D rendering of the daisy chain structure with top die connections in orange and bottom ones in blue. Note that some of the traces connect top pads while others connect bottom ones. Also, note the alternating nature of the connection.

5.3 3D Magnetic Field Imaging Case study

Two probe pads were connected to inject an AC signal of about 5 kHz into the daisy chain. We then proceeded to acquire magnetic images under the SQUID (Fig. 8a) and the GMR sensor (Fig. 8b). Figure 8c shows the corresponding optical image. The difference in resolution achieved by both sensors is clearly noticeable by comparing the images in Figure 8a and Figure 8b. Although both scans are identical in size (2000 µm x 300 µm), acquired at identical step sizes ($\Delta x = \Delta y = 1$ µm) and conditions and applying 1.7mA in both cases, the SQUID scan is acquired at about 190 µm from the surface of the top die while the GMR sensor was at about 10 µm. This factor of almost 20 reductions in scanning distance is mainly responsible for the improvement in resolution.

The increased resolution achieved by using the GMR sensor results, conversely, in lower field sensitivity, as the SQUID is more sensitive than the GMR and thus, capable of detecting equal magnetic field at larger distances compared to the GMR. For our analysis, this implies that the SQUID can easily see the feeding currents, coming from the bottom die into the microbumps and then connecting to the vias at the bottom of the structure, as sketched in Figure 7c, while the GMR will have more difficulty finding the exact path in the bottom die, separated by about 60 µm from the top current (assuming about 10 µm for the microbump height).

This can be clearly seen in Figure 8d where we plot the current density, obtained by the standard 2D inversion technique: this technique assumes the current lies in a

single layer but in reality, top and bottom currents are separated by about 60 µm. Because the intensity of the magnetic field depends inversely on distance (and linearly on current, that is the same for all segments), the 2D inverse algorithm compensates for this difference in magnetic intensity by artificially increasing the current for the top current segments relative to the bottom segments. The false color image shows higher density current in yellow and scales from red (lower intensity) to black (no current). It is clear that, although the 2D inverse from the GMR provides a good initial insight into the current path identifying the top current and also points to the presence of current in more than one level, it lacks the capability to define the bottom current path, represented just by a blur of red color linking the top current segments. Furthermore, in cases with 3 or more current levels, it is generally impossible to discern how many layers the current passes through. And finally, from the current density data in general we cannot obtain the vertical separation between current layers.

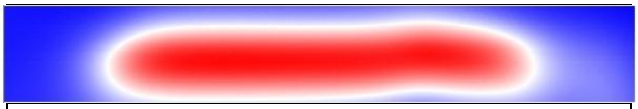

Figure 8a. *Magnetic field image acquired with a SQUID sensor at 190 µm from the surface of the top die.*

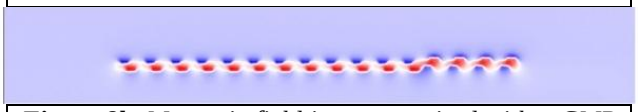

Figure 8b. *Magnetic field image acquired with a GMR sensor located at about 10 µm from the surface of the top die.*

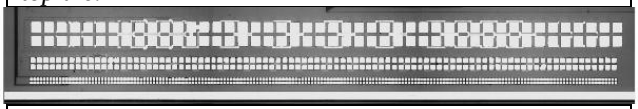

Figure 8c. *Corresponding optical image.*

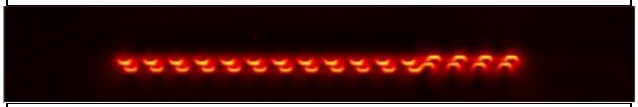

Figure 8d. *Current density obtained by the standard 2D inversion technique from the GMR data.*

5.4 3D Solver analysis of Magnetic Field

These same images where analyzed using the 3D solver technique. This technique relies uniquely on the acquired magnetic data and an initial current path that is extracted from the same acquired data by using a variety of methods developed by Neocera in collaboration with University of Maryland. Using this as a starting point, the 3D solver then adjusts the current path by computing the expected magnetic field from the proposed current path and comparing it with the acquired magnetic field data. As there are an infinite number of possible small variations to the current path, this task may seem impossible as it would require a tremendous number of computations requiring an enormous (infinite) time. However, through investigation and analysis of the magnetic field signal, we have develop a method that allows to find a solution in a manageable time and that results in a successful reconstruction of the 3D current path. Furthermore, the 3D solver also allows us to determine critical geometrical parameters, like the distance from the sensor to the top current layer (z-distance), as well as the relative vertical separation of layers.

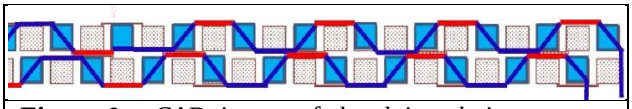

Figure 9a. *CAD image of the daisy chain structure with a sketch of the current path for clarification. Red segments are on the top die while blue ones are in the bottom die. Solid blue squares indicate TSVs transferring current form top/bottom and vice versa. Note that there is an inversion in the top/bottom alternating pattern at the location marked with the red arrow.*

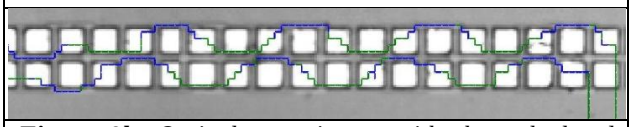

Figure 9b. *Optical scan image with the calculated current path from the 3D solver. Green lines denote current in the bottom die. Blue lines denote current in the top die. Note the inversion in the top/bottom alternating sequence marked by the red arrow. The in-fee/out-feed wires are at the bottom die.*

In order to help understanding the results of the 3D solver by comparison with the expected current path, Figure 9a shows a CAD image of the bottom layer of the daisy chain structure showing the location of the in and out current. Solid blue TSV pads show the actual structures being connected when the pin connections are powered up. Red segments are on the top die while blue ones are in the bottom die. Solid blue squares indicate TSVs transferring current form top/bottom and vice versa. Note that there is an inversion in the top/bottom alternating pattern at the location marked with the red arrow.

The results of the application of the 3D solver technique to the above scans are shown in Figure 9b. The path calculated by the 3D solver is shown overlaid on the optical image. Green lines denote current in the bottom die. Blue lines denote current in the top die. Note the inversion in the top/bottom alternating sequence marked by the red arrow.

Besides providing a much more clear identification of the 3D current and better localization accuracy, the 3D solver computes the sensor to current separation for the SQUID to be 190.64 µm. This is in excellent agreement with the top die-to distance of 190 µm for this scan, considering that the top current lies on the surface of the top die, maybe just covered by a thin passivation layer (typically of 0.5 µm thickness or less). The distance computed for the GMR scan was about 9.7 µm. In addition, the 3D solver computes a vertical separation of about 62 µm between top and bottom currents, also in excellent agreement with the expected 60 µm.

Although the solution did not totally converge and there is room for improvement in fine-tuning the distances and accuracy of the current positions, we believe this newly developed 3D solver capability is a big advance in

the use of magnetic field imaging for 3D IC fault isolation. Further work is in progress to improve the convergence time, accuracy and automation of the 3D solver.

5.5 Case Study 2: Conclusion

We show that a magnetic field imaging using a high sensitive sensor with lower resolution combined with a high resolution sensor with lower sensitivity provides highly accurate 3D information on a current path in a TSV devices structure. The applications can range from Electric Fault isolation to path finding and advanced design verifications.

6. Conclusion

We present Magnetic Field Imaging as a one-stop solution to all static Electric Fault Isolation including shorts, leakages and opens in X, Y and Z direction with sub micron accuracy. We also show that MFI can be used for advanced design verification and path finding in 3D YSV structures.

References

1. "Amkor Technology Reports Financial Results for the Fourth Quarter and Full Year 2011," Q4 and 2011 Amkor Technology, Inc. Earnings Conference Call, February 9, 2012.
2. M. Santarini, Xilinx, "2.5D ICs are more than a stepping stone to 3D ICs" Published in EE Times 3/27/2012
3. C. Maxfield, "2D vs. 2.5D vs. 3D ICs 101", Published in EE Times 4/8/2012.
4. O. Breitenstein, et al, "Microscopic lock-in thermography investigation of leakage sites in integrated circuits", Rev. Sci. Instrum. 71, 4155 (2000).
5. A. Glowacki, C. Boit, Berlin University of Technology-German and P. Perdu, CNES – France, "Optimum Si thickness for backside detection of photon emission using Si-CCD" ESREF Proceedings 2012.
6. T. Sun, G. L. Woods, M. F. Duarte, K. Kelly, C. Li, and Y. Zhang, Rice University, Houston, TX, USA "OBIC Measurements without Lasers or Raster-Scanning Based on Compressive Sensing " ISTFA Proceedings 2009
7. J. P. Wikswo, "SQUID sensors: Fundamentals, Fabrication and Applications, Chapter The Magnetic Inverse Problem for NDE", pp. 629-695, Kluwer Academic Publishers, The Netherlands, 1996.
8. E. F. Fleet, et al., "HTS scanning Microscopy of Active Circuits", IEEE Transactions on Applied Superconductivity, 9 (2): 4103 (1999).
9. D. P. Vallett, "A Comparison of Lock-in Thermography and Magnetic Current Imaging for Localizing Buried Short-Circuits", ISTFA proceedings, 2011.
10. J. Gaudestad, V. Talanov, P. C. Huang, " Space Domain Reflectometry for Opens Detection in Stacked-Die Packages", Electronic Device Failure Analysis Society (EDFAS) Magazine, August 2012, pp. 22-28
11. L. A. Knauss, et al., "Current Imaging using Magnetic Field Sensors", Microelectronics Failure Analysis Desk Reference 5th Ed., pp. 303-311 (2004).
12. J. Gaudestad, V. Talanov, N. Gagliolo, and A. Orozco, "Space Domain Reflectometry for open failure localization", Proc. 19th International Symposium Physical & Failure Analysis of Integrated Circuits (ISTFA) 2012.
13. J. Gaudestad, V. Talanov, Neocera, P. C. Huang, TSMC, "Space Domain Reflectometry for Opens Detection Location in Micro Bumps", ESREF 2012
14. A. Orozco, J. Gaudestad, N. E. Gagliolo, C. Rowlett, E. Wong, A. Jeffers, B. Cheng, F. C., Wellstood, A. B. Cawthorne and F. Infante, "3D Magnetic Field Imaging for Non-Destructive Fault Isolation, Proc. 39th International Symposium for Testing and Failure Analysis, San Jose, CA, 2013.
15. A. Orozco, "Magnetic Current Imaging in Failure Analysis", Electronic Device Failure Analysis, Vol.11 (2009), pp. 14-21.
16. J. Gaudestad, A. Orozco, V. V. Talanov, Neocera, P. C. Huang, TSMC, "Open Failure Detection in 3D Device non destructively" LSI Testing Symposium, Osaka, 2012.
17. J. Gaudestad, A. Orozco, Neocera, I. De Wolf, T. Wang, IMEC, A. Jeffers, B. Cheng, F. C. Wellstood, University of Maryland, College Park, "3D IC Analysis using Magnetic Field Imaging", Nano Testing Symposium, Osaka, 2013.